Available online at www.sciencedirect.com
SCIENCE DIRECT®
Journal of Catalysis 222 (2004) 450–460
JOURNAL OF CATALYSIS
www.elsevier.com/locate/jcat

Poisoning effect of ethylcarbazole on hydrodesulfurization of 4,6-diethyldibenzothiophene

Teh C. Ho * and Duc Nguyen [1]

Corporate Strategic Research Labs., ExxonMobil Research and Engineering Co., Annandale, NJ 08801, USA

Received 27 August 2003; revised 28 November 2003; accepted 1 December 2003

Abstract

This study aims to gain a quantitative understanding of the poisoning effect of 3-ethylcarbazole (3ECBZ) on the hydrodesulfurization (HDS) of 4,6-diethyldibenzothiophene (46DEDBT) in a fixed bed of a sulfided $CoMo/Al_2O_3–SiO_2$ catalyst. A nonequilibrium, one-parameter model reproduces experimental results and quantifies how the traveling sulfur wave, nitrogen wave, and catalyst surface interact inside the reactor as the poisoning process proceeds. While 3ECBZ's adsorptivity is about nine times that of 46DEDBT, its heteroatom removal reactivity is far lower than that of 46DEDBT. The catalyst can adsorb 3ECBZ at a rate at least 17-fold faster than it can denitrogenate. Thus even a trace amount of feed nitrogen can substantially retard the HDS rate. The model extracts adsorption and surface reaction rate constants and identifies two dimensionless groups governing the poisoning process. Fundamental and pragmatic implications of the results are discussed.

Keywords: Hydrodesulfurization; Catalyst poisoning; Modeling; Diesel fuel; Diethyldibenzothiophenes; Ethylcarbazoles

1. Introduction

In the face of ever-tightening sulfur specifications for transportation fuels, sulfur removal from transportation fuels will become increasingly important in the coming years. Currently, diesel fuel's sulfur specification in many countries is 350–500 ppmw, but future specifications may go below 10 ppm or less. Conventional hydrodesulfurization (HDS) catalysts can remove a significant fraction of the sulfur from diesel fuel. But they lack the desired activity for the HDS of alkyldibenzothiophenes having at least one substituent located at position β to the sulfur heteroatom (the 4 and 6 positions). These refractory sulfur species, collectively, may be called β-dibenzothiophenes (β-DBTs). To meet future sulfur specifications, it is necessary to desulfurize β-DBTs whose refractoriness arises from the steric hindrance around the sulfur atom [1], as exemplified by 4,6-diethyldibenzothiophene (46DEDBT) shown in Fig. 1. The variation in reactivity within β-DBTs is significant [2], and 46DEDBT is one of the most refractory β-DBTs.

There are two prevailing thoughts on the nature of the steric hindrance. One view is that the steric hindrance retards the adsorption of β-DBTs on the catalyst surface [1,3]. This implies that the rate-limiting step lies in adsorption, which then suggests an end-on adsorption mode involving bonding between the sulfur atom and the active sites. The alternate view is that the steric hindrance slows down the surface reaction for C–S bond scission [4,5]. Here the rate-limiting step lies not in adsorption, suggesting a side-on adsorption mode that involves the π-electrons of the aromatic ring. The steric effect has also been proposed to reduce the rate of oxidative addition of the C–S bond to the catalytic site [6].

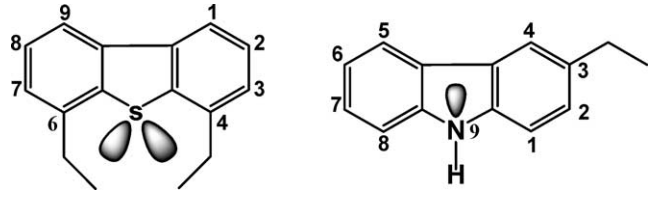

Fig. 1. Structures of 4,6-diethyldibenzothiophene and 3-ethylcarbazole.

* Corresponding author.
E-mail address: teh.c.ho@exxonmobil.com (T.C. Ho).
[1] Current address: Department of Chemical Engineering, University of Michigan, Ann Arbor, MI 48109, USA.

0021-9517/$ – see front matter
doi:10.1016/j.jcat.2003.12.010

Whether the rate-limiting step lies in adsorption or surface reaction is certainly a question of cardinal importance. A pragmatically more important question, arguably, is that of the nature of catalyst poisoning by nitrogen compounds [7–11]. A catalyst having a high intrinsic HDS activity for β-DBTs merits little if its tolerance for nitrogen poisons is unacceptably low. An essential step toward finding ways of mitigating the nitrogen poisoning effect is a quantitative investigation of the dynamics of the poisoning process, which may also shed some light on the HDS rate-limiting step. To conduct such an investigation obliges combined modeling and experimental approaches. The latter involves careful choice of model compounds and proper experimental design. Carbazoles are an excellent choice as model nitrogen compounds because they are the predominant nitrogen species in hard-to-desulfurize petroleum middle distillates (e.g., light catalytic cycle oils) [12–15]. Moreover, when refiners push diesel HDS to the ultralow sulfur regime, the process is primarily governed by the inhibiting effect of alkylcarbazoles even for not-hard-to-desulfurize feedstocks [16–18]. Experimentally, it is imperative to decouple poisoning from the HDS reaction by using a *flow* reactor under *both* transient and steady-state conditions. The thus-obtained data must be analyzed with a robust adsorption-kinetics model capable of reproducing the observed temporal transition from one steady state (say, unpoisoned state) to another steady state (poisoned state) for *both* sulfur and nitrogen species. A robust model achieves this with the fewest adjustable parameters. Since presulfided HDS catalysts generally require a long time to line out their activities and selectivities, batch autoclaves are not an ideal experimental setup for quantifying catalyst poisoning effects.

An attempt was previously made to rationalize why 46DEDBT HDS is so sensitive to even a trace amount of 3-ethylcarbazole (3ECBZ) [19]. It was posited that the structure of 46DEDBT is such that its desulfurization demands highly hydrogenative sites, dubbed β sites for the present discussion. Such special sites presumably involve specific multiplets (or ensembles) of specifically arranged adjacent sulfur vacancies whose catalytic properties depend strongly on the metals used (e.g., Co, Ni, Mo, W). They should be a small subset of catalytically active sulfur vacancy sites. Geometrically, it does not take much 3ECBZ to break up a β site. Fig. 1 shows that 3ECBE and 46DEDBT have a similar shape. Molecular shape was used to explain why fluorene is a far stronger inhibitor than anthracene and phenanthrene in the HDS of 4,6-dimethyldibenzothiophene [20].

The present work aims to gain a predictive understanding of 3ECBZ's poisoning effect on the HDS of 46DEDBT observed previously [19]. The catalyst used is a sulfided $CoMo/Al_2O_3$–SiO_2. Data obtained from steady-state and transient experiments with a flow reactor are used to construct a nonequilibrium, competitive adsorption-reaction model that quantifies what goes on in the fluid phase and on the catalyst surface. The model extracts underlying adsorption and kinetic rate constants, thus providing insights into the coupling between HDS kinetics and poisoning. Implications of the results for practical applications are discussed.

2. Experimental

2.1. Materials

The gases used were cylinder hydrogen of electrolytic grade (99.95%) and a cylinder 10% H_2S/H_2 mixture. Dodecane was analytic pure grade. Both 46DEDBT and 3ECBZ were synthesized through known procedures by an external source. A commercial $CoMo/Al_2O_3$–SiO_2 catalyst, in the form of 1/16-inch extrudates, was crushed and sieved into 20- to 40-mesh granules. Prior to use, the catalyst was sulfided at 400 °C for 1 h at atmospheric pressure with a 10% H_2S-in-H_2 mixture.

2.2. Reactors and procedures

A cocurrent fixed-bed reactor, made of a 3/8-inch i.d. 316 stainless-steel pipe, was operated isothermally in the upflow mode to avoid incomplete catalyst wetting and bypassing. Glass beads were charged in the fore and aft zones to achieve vapor-liquid equilibrium. To mitigate the axial dispersion effect, 3 g catalyst was uniformly mixed with an equal volume of glass beads in the reactor central zone. Comparative experiments showed that the diluted bed indeed gave a higher HDS level than the undiluted bed.

The liquid products were identified and quantified by GC/MS and GC using a 75% OV1/25% SW-10 fused silica capillary column. In addition, the total nitrogen was analyzed by combustion and chemiluminescence using the Antek analyzer. Due to their low concentrations, individual hydrodenitrogenation (HDN) products were not measured. The carrier solvent dodecane was essentially inert under the reaction conditions studied. The product gases were vented through a caustic scrubber followed by a wet test meter.

Table 1 lists the compositions of the feed mixtures (density = 0.72 g/cc), with the balance being dodecane.

As detailed elsewhere [19], the experiments were started with feed A (1067 ppmw total sulfur as atom) and pure hydrogen to obtain the base-case data in the absence of 3ECBZ. The conditions used were 265 °C, 2.4 WHSV (liquid weight hourly space velocity), 1.83 MPa hydrogen pressure, and 116 cc H_2/cc liquid feed. After the catalyst lined out its activity (steady state I), the reactor was switched over to feed B (1067 ppmw sulfur plus 80 ppmw nitrogen as atom) at time

Table 1
Feed compositions (wt%)

Feed	Feed A	Feed B
46DEDBT	0.8	0.8
3-Ethylcarbazole	0.0	0.112

zero under the same reaction conditions. The state of the reactor was monitored by intermittently analyzing the liquid products at the reactor outlet until the catalyst reached a new steady state (steady state II).

Besides H_2S, the main HDS products were identified to be diethylbiphenyls, diethylcyclohexylbenzenes, ethylcyclohexylbenzenes, ethylbiphenyls, ethylbenzene, and ethylcyclohexane. These products accounted for more than 98% of 46DEDBT converted. Diethylbicyclohexyl, ethylbicyclohexyl, biphenyl, and cyclohexylbenzene were present in trace amounts. Products from partial hydrogenation of 46DEDBT, if present, are negligibly small in concentration.

3. Experimental results

Fig. 2 shows the transient responses of the system to a sudden step change in the feed nitrogen content from zero to 80 ppmw. The solid curves are model predictions to be discussed later. The percentage of HDS, initially at about 70%, declines during the breakthrough period. When the system ultimately reaches steady state II after more than 50 h, the HDS level drops to about 10%. Evidently, 46DEDBT simply cannot compete with 3ECBZ for active sites. Also shown in Fig. 2 is the total nitrogen content (ppmw) of the effluent liquid as a function of the elapsed hour. The breakthrough does not occur until around the 20 h (the time when the presence of the nitrogen poison in the effluent is first detected), after which the nitrogen content of the liquid effluent takes an upward leap, giving rise to a 58% HDN at steady state II. The data shown in Fig. 2 are used to validate a mathematical model of this process.

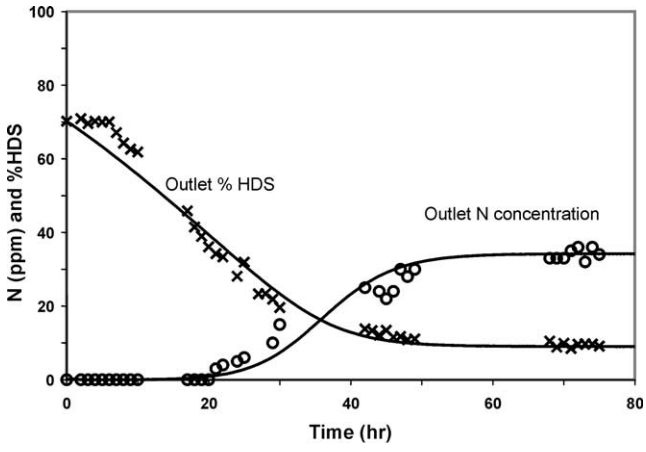

Fig. 2. Percentage of HDS and total nitrogen concentration at reactor exit as functions of elapsed time following introduction of 3-ethylcarbazole; 265 °C, 2.4 WHSV, 1.83 MPa, and 116 cc H_2/cc liquid feed. Solid curves are predicted from the nonequilibrium model.

4. Modeling of poisoning process

4.1. Full model

Our objective is to develop as simple a model as possible (fewest possible fitting parameters) and yet capture the salient features of the system. Since the HDS of 46DEDBT primarily follows the hydrogenation pathway [19], we do not distinguish the hydrogenation and hydrogenolysis sites, with the tacit assumption that 46DEDBT and 3ECBZ both adsorb and react exclusively on β sites. Nor is it unreasonable to presume that heterocycles (sulfur and nitrogen compounds) and hydrogen adsorb on different sites [21]. Other major assumptions are as follows. (A) The catalyst surface is Langmuirian. (B) All of the sulfur compounds (46DEDBT and a trace amount of hydrogenated 46DEDBT) can be lumped as a pseudo sulfur compound with the overall adsorption constant k_s, desorption constant k'_s, and the overall surface HDS rate constant k_{HDS}. Similarly, all of the nitrogen compounds (3ECBZ and hydrogenated 3ECBZs) can be lumped as a pseudo nitrogen compound, with the corresponding rate constants k_n, k'_n, and k_{HDN}. (C) HDS and HDN both take place irreversibly on the catalyst surface and hydrogen addition is not rate limiting. (D) Desorption of HDS and HDN hydrocarbon products is instantaneous. In this regard, we note that 3,3′-dimethylbiphenyl shows almost no inhibiting effect on the HDS of 4,6-dimethyldibenzothiophene [22]. (E) The inhibiting effects of H_2S and NH_3 are far smaller than that of 3ECBZ [17,23,24]. (F) Axial dispersion effect and the velocity changes due to adsorption are negligible. (G) The concentrations of sulfur and nitrogen species are constant throughout the catalyst particles. (H) The reactor is isothermal and isobaric, with negligible mass transfer effects. (I) Hydrogen partial pressure is approximately constant because of the high treat gas ratio used. The effect of molar change due to reaction is negligible. (J) Catalyst deactivation by coking is negligible. (K) Liquid feed and H_2 reach physical equilibrium before entering the catalyst bed.

Let S and N be the sulfur atom and nitrogen atom concentrations in the flowing stream (g heteroatom/cc feed), respectively. Also, let q_n and q_s be the adsorbed nitrogen and sulfur concentrations (heteroatom mass per catalyst mass), respectively. If q_m is catalyst's total capacity for adsorption on β sites, then $\theta_n = q_n/q_m$ is the fractional coverage of adsorbed nitrogen on β sites. Here we follow the industrial practice by using the mass of the heteroatom in the units of S, N, and q_m.

With the above assumptions, the transient response of the system after introducing 3ECBZ (time $t > 0$) is described by the following plug flow, one-dimensional model.

(i) S mass balance in the fluid phase

$$v\frac{\partial S}{\partial z} + \varepsilon\frac{\partial S}{\partial t} + (1-\varepsilon)\rho_p\left[k_s S(q_m - q_n - q_s) - k'_s q_s\right] = 0. \quad (1)$$

(ii) S mass balance in the solid phase

$$\frac{\partial q_s}{\partial t} = k_s S(q_m - q_n - q_s) - k'_s q_s - k_{HDS} q_s. \quad (2)$$

(iii) N mass balance in the fluid phase

$$v\frac{\partial N}{\partial z} + \varepsilon\frac{\partial N}{\partial t} + (1-\varepsilon)\rho_p\left[k_n N(q_m - q_n - q_s) - k'_n q_n\right] = 0. \quad (3)$$

(iv) N mass balance in the solid phase

$$\frac{\partial q_n}{\partial t} = k_n N(q_m - q_n - q_s) - k'_n q_n - k_{HDN} q_n. \quad (4)$$

Here ε, ρ_p, and v are bed void fraction, catalyst bulk density (in sulfided form), and the superficial fluid velocity based on empty reactor, respectively. The average fluid velocity in the interstices between particles is v/ε. The symbols are defined under Nomenclature if not stated otherwise.

The foregoing model, in the limit $\partial/\partial t \to 0$, must also describe the system behaviors at steady states I and II. As will be seen later, only by combining the transient and steady-state experiments, may one arrive at a robust model. Before proceeding further, it pays to simplify the problem. As a staring point, we construct perhaps the most compact model by invoking the quasi-equilibrium and quasi-steady-state approximations, as commonly done in kinetic analysis.

4.2. Quasi-equilibrium and quasi-steady-state model

We assume that $k_{HDS} \ll (k_s S_f, k'_s)$ and $k_{HDN} \ll (k_n N_f, k'_n)$, so adsorption and desorption are in quasi-equilibrium for both sulfur and nitrogen species. We further suppose that the time scales for adsorption and desorption are so much shorter than the reactor residence time ($\varepsilon L/v$) that the catalyst surface quickly relaxes to a quasi-steady state ($\partial q_s/\partial t \approx 0$ and $\partial q_n/\partial t \approx 0$) as the 3ECBZ-containing feed travels down the bed after the startup of the poisoning experiment. These two assumptions reduce Eqs. (2) and (4) to the following algebraic equations relating the solid phase to the fluid phase, that is, the Langmuir isotherm in a competitive environment,

$$q_s = \frac{K_s q_m S}{1 + K_n N + K_s S}, \quad (5)$$

$$q_n = \frac{K_n q_m N}{1 + K_n N + K_s S}, \quad (6)$$

where $K_n = k_n/k'_n$ and $K_s = k_s/k'_s$ are the adsorption equilibrium constants. To be consistent with the observed exponential decay of the reactor sulfur profile at steady state I [19], we impose that $K_s \ll K_n$. The result is the following much simplified model:

$$v\frac{\partial S}{\partial z} + \varepsilon\frac{\partial S}{\partial t} = -\frac{(1-\varepsilon)\rho_p k_{HDS} K_s q_m S}{1 + K_n N}, \quad (7)$$

$$v\frac{\partial N}{\partial z} + \varepsilon\frac{\partial N}{\partial t} = -\frac{(1-\varepsilon)\rho_p k_{HDN} K_n q_m N}{1 + K_n N}. \quad (8)$$

The boundary conditions at the reactor inlet $z = 0$ ($t > 0$) are $S = S_f$ and $N = N_f$, with S_f and N_f being the concentrations of the sulfur and nitrogen atoms in the liquid feed, respectively. The initial conditions $t = 0$ ($z \geqslant 0$) are $N = 0$ and $S = \widehat{S}(z)$, where $\widehat{S}(z)$ is the reactor sulfur profile at steady state I. Besides K_n, the model is characterized by two lumped parameters: $k_{HDS} K_s q_m$ and $k_{HDN} K_n q_m$. All of them can be determined from steady state I and II data.

Setting $\partial S/\partial t = \partial N/\partial t = 0$ in Eqs. (7) and (8) yields the familiar equilibrium-based Langmuir–Hinshelwood model for steady state II, one that has been used extensively in the literature for modeling catalyst poisoning. This classical model invokes both the equilibrium and the steady-state assumptions.

Eqs. (7) and (8) can be solved analytically by the method of characteristics [25], as detailed in Appendix A. The equilibrium and steady-state assumptions imply that the adsorption of the nitrogen poison is exceedingly fast and strong ($\theta_n \approx 1$). As a result, as depicted in Fig. 3a which shows the movement of θ_n, there are two sharp moving zones in the bed. Zone A (upstream, shaded area) is completely poisoned, whereas zone B is poison free. The poison wave moves at the speed of the carrier solvent v/ε. Fig. 3b shows that zones A and B are separated by line 0Q ($t = \varepsilon z/v$) when projected onto the t–z plane. Zone A ($t > \varepsilon z/v$) is characterized by the parallel lines emanating from $z = 0$, where the poison is constantly supplied at the concentration N_f (and sulfur at S_f). This zone feels the nitrogen disturbances, which propagate from the reactor inlet ($z = 0$) along the parallel *characteristic* lines of slope ε/v (see the arrow in Fig. 3b). Zone *B* ($t < \varepsilon z/v$) has not yet felt the nitrogen attack and hence is still governed by the initial condition $t = 0$ through "information" propagation along the *characteristic* lines emanat-

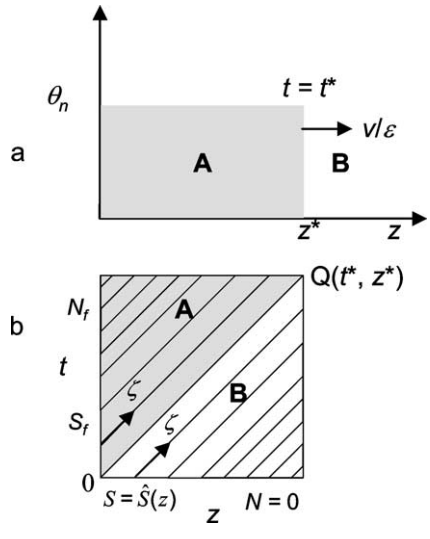

Fig. 3. (a) Movement of θ_n wave inside the reactor. Zone A is poisoned, while zone B is poison free. (b) All characteristics, whether emanating from $z = 0$ or $t = 0$, are straight lines of the same slope ε/v. Zone A is under the influence of the boundary condition at $z = 0$, while zone B is under the influence of the initial condition at $t = 0$. The arrow indicates the characteristic direction for information propagation.

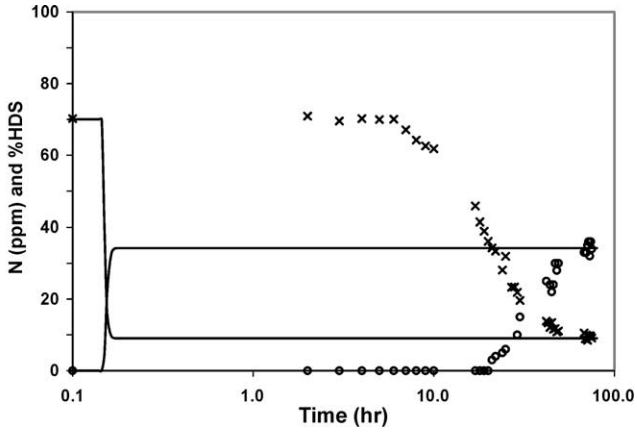

Fig. 4. Percentage of HDS (×) and total nitrogen concentration (o) at reactor exit as functions of elapsed time (log scale); 265 °C, 2.4 WHSV, 1.83 MPa, and 116 cc H_2/cc liquid feed. Solid lines are predicted from the quasi-equilibrium and quasi-steady-state model.

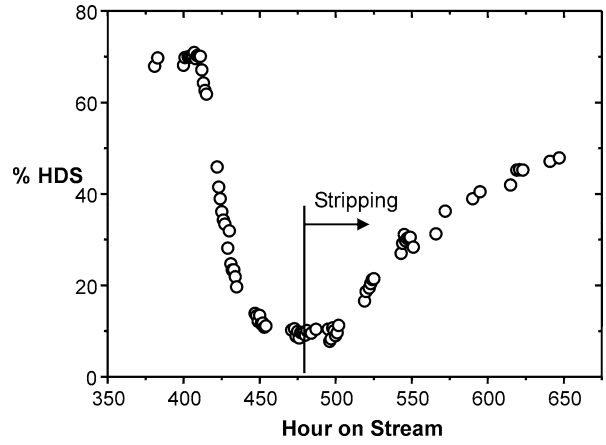

Fig. 5. Percentage HDS vs elapsed hour after introduction of feed B at 400 h; 1.83 MPa, 265 °C, 2.4 WHSV, 116 cc H_2/cc liquid feed. The vertical line indicates the beginning of the stripping experiments using feed A [19].

ing from $t = 0$ at which $S = \widehat{S}(z)$ and $N = 0$. This physical picture greatly simplifies the mathematical analysis (Appendix A).

The structure of the model is such that S, N, and θ_n behave as sharp waves moving at the fluid speed v/ε. So the calculated breakthrough time is nothing but the fluid residence time. As Fig. 4 shows, the model simply cannot describe the breakthrough behavior of the system. Yet it surely can be made to match the steady-state data. Thus the key message here is that rate constants determined from steady-state experiments may not be able to describe reactor performance under transient conditions. Robust rate constants should be determined from both transient and steady-state experiments.

4.3. Quasi-equilibrium model

The forgoing discussion obviously invites the question: Why not keep the catalyst capacity term by relaxing the quasi-steady-state assumption? Appendix B shows the resulting model, which can be solved analytically as well [25]. We do not show the results except to say that the poison wave does move far slower than the fluid velocity. However, the model predicts a much steeper rise in the exit nitrogen concentration after the breakthrough. Moreover, it cannot predict the nitrogen concentration at steady state II because surface HDN is overlooked. In what follows we develop perhaps the simplest nonequilibrium model that rectifies the problem at hand.

4.4. Nonequilibrium model

The results reported in [19] offer some clues as to how we may simplify matters. First, the reactor sulfur profile at steady state I is exponential, suggesting that 46DEDBT may sparsely occupy the active sites even in the absence of 3ECBZ. Despite the low occupancy, the overall HDS rate is respectably fast (70% HDS), hinting that the surface HDS rate may be quite fast relative to the desorption rate. We thus assume that $q_s \ll q_m$ and $k_{HDS} \gg k'_s$. Second, as shown in Fig. 5 [19], adsorbed nitrogen species are quite sticky and do not desorb easily. In fact, it does not seem possible to completely recover the lost HDS activity after stripping with feed A for a long time. Others have also observed this high stickiness of five-membered nitrogen heterocycles [15,26]. It seems then safe to assume $k_n \gg k'_n$. Thirdly, given the reasonably high HDN of 58%, we suppose that $k_{HDN} \gg k'_n$. Finally, Fig. 2 indicates that 46DEDBT is no match for 3ECBZ in competitive adsorption, implying $k_n \gg k_s$. Similarly, q_s is low even in the absence of 3ECBZ, indicating $q_s \ll q_n$ in the presence of 3ECBZ. That q_s is small at both steady states I and II means that its impact on the dynamics of the poisoning process is insignificant.

The foregoing order-of-magnitude analysis leads to the following reduced model:

$$v\frac{\partial S}{\partial z} + \varepsilon\frac{\partial S}{\partial t} + (1-\varepsilon)\rho_p k_s S(q_m - q_n) = 0, \tag{9}$$

$$v\frac{\partial N}{\partial z} + \varepsilon\frac{\partial N}{\partial t} + (1-\varepsilon)\rho_p k_n N(q_m - q_n) = 0, \tag{10}$$

$$\frac{\partial q_n}{\partial t} = k_n N(q_m - q_n) - k_{HDN} q_n. \tag{11}$$

The model serves as the surrogate of the full model in the limits $k'_n \to 0$, $k'_s \to 0$, and $q_s \to 0$. It has four parameters (k_{HDN}, k_n, k_s, and q_m), vs seven in the full model. Only one of the four parameters is adjustable due to steady-state constraints, as discussed in the next two sections.

4.4.1. Boundary conditions

The corresponding boundary conditions at $z = 0$ ($t > 0$) are $S = S_f$, $N = N_f$, and

$$\frac{d\tilde{q}_n}{dt} = k_n N_f(q_m - \tilde{q}_n) - k_{HDN}\tilde{q}_n, \tag{12}$$

where $\tilde{q}_n = q_n$ at $z = 0$. Equation (12) upon integration with the initial condition $\tilde{q}_n(0) = 0$ gives

$$\tilde{q}_n(t) = \frac{k_n N_f q_m [1 - e^{-(k_n N_f + k_{HDN})t}]}{k_n N_f + k_{HDN}} \quad \text{at } z = 0. \tag{13}$$

4.4.2. Initial conditions

The initial conditions for the model correspond to the steady state of the reactor prior to poisoning (steady state I). Thus, at $t = 0$ ($z \geqslant 0$), we have

$$N = q_n = 0 \tag{14}$$

and

$$v\frac{d\widehat{S}}{dz} + (1-\varepsilon)\rho_p k_s q_m \widehat{S} = 0, \tag{15}$$

where $S = \widehat{S}(z)$ at $t = 0$. Equation (15) can be readily integrated with the reactor inlet condition $\widehat{S}(0) = S_f$ to yield

$$\widehat{S}(z) = S_f \exp\left[-\frac{(1-\varepsilon)\rho_p k_s q_m}{v} z\right]. \tag{16}$$

This exponential decay, corresponding to the reactor sulfur profile at steady state I, is what was observed experimentally [19]. Here the extent of HDS is dictated by 46DEDBT adsorption. Since WHSV $= v/[(1-\varepsilon)\rho_p L]$, the apparent pseudo-first-order HDS rate constant measured previously [19] is $k_{app} = k_s q_m$.

Setting $z = L$ in Eq. (16) gives S_{p1}, the total sulfur concentration in the liquid product at steady state I. The result is a relationship between k_s and q_m

$$k_s = \frac{v \ln(S_f/S_{p1})}{(1-\varepsilon)\rho_p q_m L}. \tag{17}$$

Finally, with the boundary and initial conditions, Eqs. (9) to (11) were solved numerically by using an implicit finite difference scheme.

4.5. Steady state II

In the limit $t \to \infty$, Eqs. (9)–(11) define steady state II at which $S = \overline{S}(z)$ and $N = \overline{N}(z)$. Dividing Eqs. (9) by (10) gives the relation $d\overline{S}/d\overline{N} = (k_s/k_n)(\overline{S}/\overline{N})$ from which k_n is related to k_s as

$$k_n = k_s \frac{\ln(N_{p2}/N_f)}{\ln(S_{p2}/S_f)}, \tag{18}$$

where S_{p2} and N_{p2} are the total sulfur and nitrogen concentrations in the effluent liquid at steady state II.

At steady state II, Eq. (11) becomes

$$\bar{q}_n(z) = \frac{k_n \overline{N}(z)}{k_n \overline{N}(z) + k_{HDN}} q_m. \tag{19}$$

In the absence of HDN, $\bar{q}_n = q_m$; i.e., all of the active sites are occupied by nitrogen species. Substituting Eq. (19) into Eq. (10) gives

$$v\frac{d\overline{N}}{dz} + (1-\varepsilon)\rho_p k_n q_m \frac{k_{HDN}\overline{N}}{k_n \overline{N} + k_{HDN}} = 0, \tag{20}$$

with $N = N_f$ at $z = 0$. Upon integration and rearrangement, Eq. (20) becomes

$$k_{HDN} = \frac{(N_f - N_{p2})k_n v}{v \ln(N_{p2}/N_f) + (1-\varepsilon)\rho_p q_m L k_n}. \tag{21}$$

This equation allows k_{HDN} to be determined from q_m and the HDN data obtained at the reactor outlet at steady state II.

4.6. Property ratios

From Eqs. (18) to (20), one can identify two dimensionless groups p and g that govern the poisoning behavior at steady state II. They are

$$p \equiv \frac{k_s}{k_n} = \frac{\ln(S_{p2}/S_f)}{\ln(N_{p2}/N_f)}, \tag{22}$$

$$g \equiv \frac{k_n N_f}{k_{HDN}} = \frac{N_f \ln(N_{p2}/N_f)}{(N_f - N_{p2})}\left(1 - \frac{\ln(S_{p1}/S_f)}{\ln(S_{p2}/S_f)}\right). \tag{23}$$

Hence p is the adsorptivity ratio reflecting the intrinsic adsorption affinity of the sulfur species relative to that of the nitrogen poison. The parameter g is the ratio of nitrogen adsorption rate to surface HDN rate. Put differently, it is the ratio of HDN time scale ($1/k_{HDN}$) to nitrogen adsorption time scale ($1/k_n N_f$). As such, g is an index of poisoning intensity. Both p and g are functions of catalyst properties. For a given catalyst, p and g depend on temperature. Other dimensionless groups are provided in Appendix C.

4.7. Parameter estimation

The parameter estimation was carried out with constraints derived from steady-state experiments ($\widehat{S}$, $\overline{N}$, and $\overline{S}$). The observed breakthrough time allows an initial estimate of q_m. Eqs. (17), (18), and (21) were used to calculate k_s, k_n, and k_{HDN}, respectively. The corresponding best q_m value was then obtained from a least-squares fit to the transient HDS and HDN data shown in Fig. 2. The resulting q_m was then used to estimate an improved set of k_s, k_n, and k_{HDN} values, which was used to calculate an improved q_m. This iterative process continued until the system converges. In essence, q_m is the only adjustable parameter—which was estimated from *both* the transient HDS and HDN data. Meeting this rather stringent requirement greatly enhances the robustness of the model. In the regression we account for the travel time for feed B to reach the inlet of catalyst bed after the reactor is switched from feed A to feed B. The numerical values of physical properties and operating parameters are listed under Nomenclature.

5. Results

5.1. Comparison with experiment

The solid curves in Fig. 2 are model predictions, which compare well with measured nitrogen exit concentration and

the percentage of HDS as functions of elapsed hour after introducing the 3ECBZ-containing feed. The model also satisfactorily predicts the nitrogen breakthrough time of about 20 h. However, it underpredicts the HDS level for the initial part (0–5 h) of the prebreakthrough period. Within this short "induction" period the exit percentage HDS actually remains fairly constant. Accepting the validity of the Langmuir surface assumption, we may attribute this induction time to the following possible physical situations that are not considered in the model. Initially, it is tough for "free-falling" nitrogen species to hit a "target" because the β sites are sparsely occupied by sulfur species. This severely limits the poisoning power of 3ECBZ. Second, some of the partially hydrogenated 3ECBZs (e.g., tetrahydro-3ECBZ and hexahydro-3ECBZ) are likely more inhibiting [21]. The slowness of the hydrogenation rate [21,27] means that it takes time to build up an effective poison pool on the catalyst surface. The third possible situation is that nitrogen species initially fall on non-β sulfur vacancy sites, which greatly outnumber the β sites. Finally, the acidity of the Al_2O_3–SiO_2 support might play a role as well. It was considered unnecessary to refine the model to include this initial transient effect in terms of return on effort expended, since the one-parameter model in hand already captures the dominant features of the system.

5.2. Parameter values

The fit shown in Fig. 2 corresponds to the parameters listed in Table 2. In addition, we note that $q_n \gg q_s$ and that the HDS and HDN levels are comparable (70% vs 58% at steady states I and II, respectively). It follows that $k_{HDS} \gg k_{HDN} \gg k'_n$. Also, $k_{HDS} \gg k'_s$, $p = 0.11$, and $g = 17.4$.

As a consistency test, the value of $k_s q_m$ from Table 2 gives $k_{app} = 2.87$ $cc_{liquid\ feed}/(g_{cat}\,h)$, compared well with 2.73 $cc_{liquid\ feed}/(g_{cat}\,h)$ obtained previously [19]. This further suggests that our model and its kinetic parameters adequately represent the system at hand.

5.3. Dynamic features

Armed with the model parameters, we now look at the spatiotemporal behavior of the system. Fig. 6 shows the fractional sulfur concentration (S/S_f) in the fluid phase as a function of bed position at successive elapsed times. Initially ($t = 0$ h), the reactor sulfur profile in the absence of 3ECBZ shows an exponential decline. Subsequently, the fluid sulfur content increases as the concentration wave travels toward the reactor outlet. The advancing sulfur front is not in rapid adsorption–desorption equilibrium with the active sites. In all the figures to follow, the wave labeled with asterisks is for $t = 20$ h, approximately corresponding to the breakthrough time. After 30 h of nitrogen attack, the majority of the active sites in the bed are poisoned; the bulk of 46DEDBT stays in the fluid phase as a "bystander." As a result, the sulfur profile remains nearly flat and becomes only slightly concave downward near the reactor outlet where some active sites have not yet been poisoned at that moment. The sulfur concentration in reactor effluent increases as the poisoning proceeds.

Table 2
Values of model parameters

k_s, $cc/(g_s\,s)$	0.21
k_n, $cc/(g_n\,s)$	1.91
k_{HDN}, s^{-1}	6.32×10^{-6}
q_m, g_s or g_n/g_{cat}	0.0038

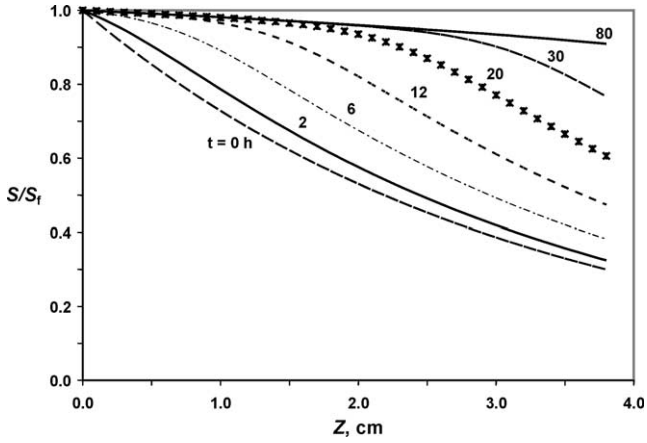

Fig. 6. Predicted moving sulfur concentration front S/S_f for different elapsed times.

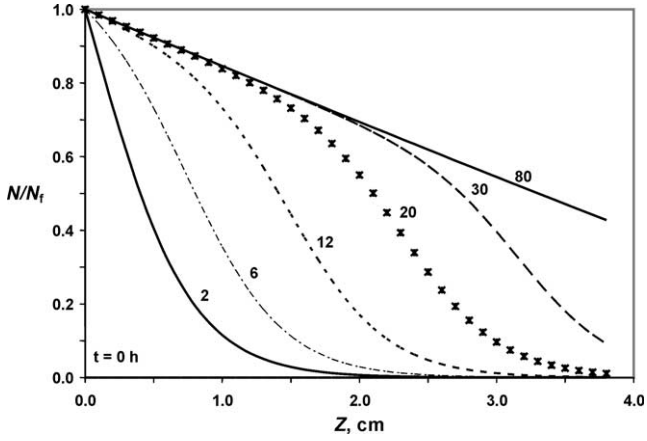

Fig. 7. Predicted moving nitrogen concentration front N/N_f for different elapsed times.

The speed with which the nitrogen wave travels through the bed is much slower than the superficial velocity of the carrier solvent. Fig. 7 shows multiple snapshots of fractional nitrogen concentration (N/N_f) in the fluid phase resulting from coupled adsorption and HDN. The moving front is accompanied by a decreasing N/N_f due to HDN whose rate plays a pivotal in the poisoning process. The model must account for surface HDN reaction; otherwise, it would not predict the nitrogen breakthrough curve *and* the steady-state nitrogen concentration.

Fig. 8 shows the fractional coverage of adsorbed nitrogen θ_n as a function of bed length at different elapsed times. The adsorption-reaction wave moves slowly toward the re-

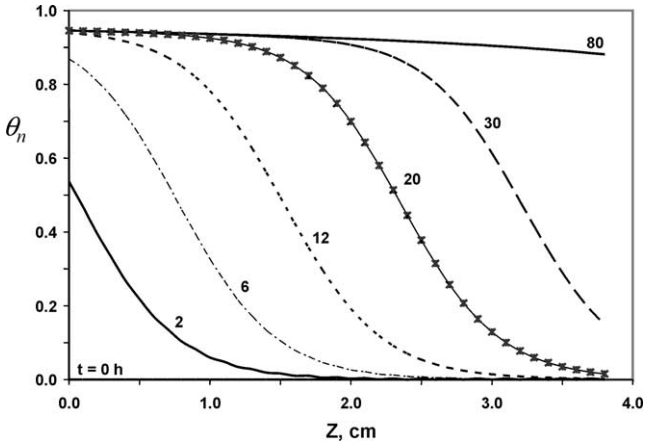

Fig. 8. Predicted fractional site coverage by adsorbed nitrogen, θ_n, for different elapsed times.

actor exit. At small t, the catalyst in the upstream section of the bed partially depletes its β sites due to nitrogen uptake. In the downstream section, the β sites are sparsely occupied by sulfur species and virtually free of adsorbed nitrogen species. For intermediate t, the catalyst near the reactor inlet gives up almost all its β sites for 46DEDBT HDS, whereas that near the outlet partially gives up its β sites for HDS. When t exceeds the breakthrough time, almost all of the β sites are blocked off by nitrogen species.

6. Discussion

6.1. Rate-limiting step

As noted before, there has been no agreement on whether the steric hindrance retards the adsorption of 46DEDBT or the C–S bond scission. The latter implies that the surface reaction is the rate-limiting step. The picture emerging from the present modeling study is that even in the absence of 3ECBZ, the adsorption of 46DEDBT is far slower than the surface HDS rate under the conditions studied. In fact, the surface HDS reaction is so fast that the desorption of 46DEDBT becomes kinetically irrelevant over the time scale of interest.

If 46DEDBT adsorption takes the end-on mode, it is not hard to see why the adsorption is rate limiting given the steric crowdedness around the sulfur atom. But it is not obvious why this should be the case if the adsorption is side on. One possible rationalization is to posit that the number of β sites on the present catalyst is so few that 46DEDBT has to "fish" for them. Once a 46DEDBT molecule is adsorbed and hydrogenated, steric hindrance becomes significantly weakened and hence a rapid removal of the sulfur atom. The consequence is that the coverage of 46DEDBT on β sites is very low. This proposition suggests that 46DEDBT may not be inherently more refractory than DBT—if a catalyst has a sufficiently high surface concentration of the required type of active sites that can accommodate 46DEDBT for its initial adsorption. Landau et al. [28] reported that 4,6-dimethyldibenzothiophene desulfurizes faster than DBT on a sulfided NiW/SiO_2 catalyst; the reverse is true on a $CoMo/Al_2O_3$ catalyst. The toluene hydrogenation activity of NiW/SiO_2 is 10 times that of $CoMo/Al_2O_3$.

For perspective, we note that the poisoning effect of 3ECBZ is less pronounced in the HDS of DBT [19]. A reasonable conjecture seems that 46DEDBT demands a high degree of site specificity for its sulfur removal. This is not the case with DBT, which can desulfurize on both β and non-β sites.

As a final note, the heats of chemisorption of 4-methyldibenzothiophene ($\sim$ 19–20 kcal/mol) and 4,6-dimethyldibenothiophene ($\sim$ 21 kcal/mol) were reported to be higher than that of DBT ($\sim$ 10 kcal/mol) over commercial $CoMo/Al_2O_3$ and $NiMo/Al_2O_3$ catalysts at 190–340 °C and 5 MPa hydrogen pressure [29]. This result has been taken as indicating that the adsorption of β-DBTs is not hindered. It must be pointed out, however, that here the heats of chemisorption were solely calculated from steady-state HDS experiments using an equilibrium-based Langmuir–Hinshelwood model. Such model, as shown earlier, may not reflect physical reality.

6.2. 46DEDBT vs 3ECBZ

The forgoing results say that a tiny fraction of the β sites gives a 70% HDS at steady state I, vs a 58% HDN over a lot of β sites at steady state II. This indicates that 46DEDBT and 3ECBZ have vastly different adsorptivities and reactivities. Thus, the surface turnover rate for the HDS of 46DEDBT is orders of magnitude greater than that for the HDN of 3ECBZ. On the other hand, 46DEDBT has a far weaker affinity for β sites than 3ECBZ ($p = 0.11$). The catalyst can adsorb 3ECBZ at a rate at least 17-fold faster than it can denitrogenate 3ECBZ ($g = 17.4$). The only similarity between 46DEDBT and 3ECBZ is that their desorption rates are kinetically insignificant over the poisoning time scale. The consequence of all this is that in a flow reactor almost all of the β sites can eventually be blocked off by nitrogen species ($\theta_n \approx 1$). This explains why even a trace amount of 3ECBZ can have a huge impact on the HDS of 46DEDBT [19].

6.3. Mitigation of inhibiting effects

As noted, g is an index of the poisoning intensity that can be measured through Eq. (23). For catalyst design, it is highly desirable to correlate g with catalyst properties (e.g., metal composition and support type) using such techniques as chemomtrics [24]. A glance at Eq. (C.6) in Appendix C reveals that the nitrogen uptake θ_n is of order unity when $g \gg 1$ and of order g when $g \ll 1$. A highly adsorptive poison by its very nature implies a high g. For typical petroleum middle distillates over commercial catalysts, g is generally greater than 10, as is the case here. Thus, a big challenge in the HDS of β-DBTs is how to accomplish $g \ll 1$. One may

think of changing the catalyst morphology to decrease k_n. The key then is how to achieve this without hurting the adsorption of β-DBTs. Decreasing k_n through modifying the electronic and steric characteristics of carbazole species has not yet shown any promise [19]. One option is to vastly improve the HDN activity. Since k_{HDN} scales linearly with N_f for a constant g (Eq. (23)), a 10-fold increase in k_{HDN} means a 10-fold increase in the tolerance for the feed nitrogen level at the same degree of poisoning. Adjusting reaction temperature can also lower g because k_n and k_{HDN} should in general have different temperature responses. There is voluminous patent literature on removing organonitrogen species from petroleum distillates via various separation schemes (adsorption, extraction, etc.).

7. Concluding remarks

One of the most important issues in the deep HDS of diesel fuel is how β-DBTs interact with alkylcarbazoles [16–18]. In an early work [19] we assembled a plethora of experimental evidence that 3ECBZ is a strong poison to the HDS of 46DEDBT. In this study, through a hierarchical modeling approach, we gain a better quantitative understanding of the dynamic interactions among 46DEDBT, 3ECBZ, and the catalyst surface. To reproduce the data obtained from both steady-state and transient experiments, the one-parameter model developed here does not invoke the usual quasi-equilibrium or quasi-steady-state assumptions. It identifies important parameters governing the poisoning process and sheds some light on the fundamentals of deep HDS catalytic chemistry and kinetics. On the practical side, the results of the present study provide some guidance as to how to mitigate the poisoning effect of alkylcarbazoles, which are found to be highly adsorptive and refractory. The adsorption and kinetic constants extracted from the model should be useful for both catalyst design and process modeling and control. In the latter case, enhanced mechanistic kinetics can be incorporated into the model.

Nomenclature

g	$k_n N_f / k_{HDN}$
k_{HDS}	Surface HDS rate constant (1/s)
k_{HDN}	Surface HDN rate constant (1/s)
k_n	Adsorption rate constant for nitrogen ($cc_{feed}/(g_n\ s)$)
k_s	Adsorption rate constant for sulfur ($cc_{feed}/(g_s\ s)$)
k'_n	Desorption rate constant for nitrogen (1/s)
k'_s	Desorption rate constant for sulfur (1/s)
K_n	Nitrogen adsorption equilibrium constant (cc_{feed}/g_n)
K_s	Sulfur adsorption equilibrium constant (cc_{feed}/g_s)
L	Reactor length (3.82 cm)
N	Concentration of nitrogen atom in the fluid phase (g_n/cc_{feed})
n	N/N_f, Appendix C
N_f	Feed nitrogen atom concentration (80 ppm as N atom) (g_n/cc_{feed})
$\overline{N}$	N at steady state II (g_n/cc_{feed})
p	Selectivity factor defined in Eq. (22)
q_m	Catalyst maximum site capacity (g_s or N/g_{cat})
q_s	Concentration of adsorbed sulfur atom on catalyst (g_s/g_{cat})
q_n	Concentration of adsorbed nitrogen atom on catalyst (g_n/g_{cat})
$\tilde{q}_n$	q_n at the reactor inlet
S	Concentration of sulfur atom in the fluid phase (g_s/cc_{feed})
S_f	Sulfur atom concentration in feed liquid (g_s/cc_{feed})
$\overline{S}$	S at steady state II
$\widehat{S}$	Sulfur concentration in the fluid phase at steady state I (g_s/cc_{feed})
s	S/S_f, Appendix C
t	Time
v	Superficial velocity (0.0021 cm/s)
z	Axial distance from the entrance of the reactor (cm)

Greek symbols

α	Time constant ratio defined in Appendix C
ε	Bed void fraction (0.3)
γ	Time constant ratio defined in Appendix C
η	Defined in Eq. (C.9)
μ	Time constant ratio defined in Appendix C
θ_n	q_n/q_m, fractional coverage of adsorbed nitrogen
ρ_p	Sulfided catalyst packing density in the bed (1.15 g/cc)
τ	$t/(L\varepsilon/v)$, Appendix C
ζ	Characteristic coordinate, Appendix A.

Acknowledgment

Duc Nguyen from the University of Michigan acknowledges a summer internship supported by ExxonMobil Research and Engineering Co.

Appendix A. Quasi-equilibrium and quasi-steady-state model

One can get a good idea of what the solution looks like from Fig. 3b, which shows the parallel characteristic lines of slope ε/v. The behaviors of S and N in zone A are time invariant because they are governed by the constant boundary conditions $N = N_f$ and $S = S_f$ at $z = 0$. One then can simply use the mass balance equations at steady state II to find S and N in this zone. Since zone B has not felt the nitrogen attack, so $N \equiv 0$ because $N = 0$ at $t = 0$. And the sulfur concentration, while being displaced, decays exponentially.

In what follows we obtain the concentration waves S and N from the method of characteristics.

For zone A ($t/\varepsilon > z/v$), we change the original (t, z) coordinate to $\zeta = z/v$ and $t_o = t - \varepsilon z/v$, where ζ is the characteristic coordinate. We do so to reflect the fact that zone A is under the influence of the boundary condition $z = 0$, since $\zeta = 0$ implies $z = 0$ and $t = t_o$, where t_o is the free time parameter along $z = 0$. It can be shown that Eqs. (7) and (8) along the characteristic direction become

$$\frac{dS}{d\zeta} = -\frac{(1-\varepsilon)\rho_p k_{HDS} K_s q_m S}{1 + K_n N}, \tag{A.1}$$

$$\frac{dN}{d\zeta} = -\frac{(1-\varepsilon)\rho_p k_{HDN} K_n q_m N}{1 + K_n N}. \tag{A.2}$$

The boundary conditions are $S = S_f$ and $N = N_f$ at $\zeta = 0$. Eqs. (A.1) and (A.2) are nothing but the governing equations for steady state II, as alluded to earlier. Dividing Eq. (A.1) by Eq. (A.2) and carrying out the integration give a power-law relation between S and N as follows (similar to Eq. (18)):

$$\frac{S}{S_f} = \left(\frac{N}{N_f}\right)^{(k_{HDS}K_s/k_{HDN}K_n)}. \tag{A.3}$$

Substituting Eq. (A.3) into Eq. (A.1) and performing the integration yield

$$\frac{N}{N_f}\exp(K_n N_f) = \exp\left(-\frac{(1-\varepsilon)\rho_p k_{HDN} K_n q_m}{v} z\right). \tag{A.4}$$

For zone B ($t/\varepsilon < z/v$), the governing mass balance equations remain the same as Eqs. (A.1) and (A.2) if we let $\zeta = t/v$ and $z_o = z - vt/\varepsilon$. When $\zeta = 0$, then $t = 0$ and $z = z_o$, reflecting that this zone is governed by the initial condition $t = 0$, with z_o being the free distance parameter. Since here $N = 0$ at $\zeta = 0$, so Eq. (A.2) has the trivial solution $N \equiv 0$. With $S = \widehat{S}(z_o)$ at $\zeta = 0$, Eq. (A.1) can be integrated to give

$$S = \widehat{S}\left(z - \frac{vt}{\varepsilon}\right)\exp\left(-\frac{(1-\varepsilon)\rho_p k_{HDS} K_s q_m}{\varepsilon} t\right), \tag{A.5}$$

where $\widehat{S}$, an exponential decreasing function, satisfies the mass balance equation at steady state I, namely,

$$v\frac{d\widehat{S}}{dz} = -(1-\varepsilon)\rho_p k_{HDS} K_s q_m \widehat{S}. \tag{A.6}$$

Appendix B. Quasi-equilibrium model

Here for simplicity we consider the limiting case $k_{HDS} \to 0$, $k_{HDN} \to 0$, and $q_s \to 0$, while keeping the catalyst capacity term $\partial q_n/\partial t$. We then have the following model

$$v\frac{\partial S}{\partial z} + \varepsilon\frac{\partial S}{\partial t} + (1-\varepsilon)\rho_p k_s S(q_m - q_n) = 0, \tag{B.1}$$

$$v\frac{\partial N}{\partial z} + \varepsilon\frac{\partial N}{\partial t} + (1-\varepsilon)\rho_p\left[k_n N(q_m - q_n) - k'_n q_n\right] = 0, \tag{B.2}$$

$$\frac{\partial q_n}{\partial t} = k_n N(q_m - q_n) - k'_n q_n. \tag{B.3}$$

The above system of equations is subject to the usual initial and boundary conditions. Eqs. (B.2) and (B.3) are self-contained. The model is essentially adsorptive in nature.

Appendix C. Scaling analysis for nonequilibrium model

The governing equations are made dimensionless by using the following scaled variables: $s = S/S_f$, $n = N/N_f$, $\xi = z/L$, $\tau = t/(L\varepsilon/v)$, and $\theta_n = q_n/q_m$. The system of mass balance equations then becomes

$$\frac{\partial s}{\partial \xi} + \frac{\partial s}{\partial \tau} + \eta s(1-\theta_n) = 0, \tag{C.1}$$

$$\frac{\partial n}{\partial \xi} + \frac{\partial n}{\partial \tau} + \mu n(1-\theta_n) = 0, \tag{C.2}$$

$$\frac{\partial \theta_n}{\partial \tau} = \alpha n(1-\theta_n) - \gamma\theta_n. \tag{C.3}$$

At steady state II, the system is defined by the following equations:

$$\frac{d\bar{s}}{d\xi} + \frac{\eta\bar{s}}{1+g\bar{n}} = 0, \tag{C.4}$$

$$\frac{d\bar{n}}{d\xi} + \frac{\mu\bar{n}}{1+g\bar{n}} = 0, \tag{C.5}$$

$$\theta_n = \frac{g\bar{n}}{1+g\bar{n}}. \tag{C.6}$$

It follows from Eqs. (C.4) and (C.5) that $\bar{s} = \bar{n}^{\eta/\mu} = \bar{n}^p$. Also, $g = [(1/k_{HDN})/(1/k_n N_f)]$ = (time scale for HDN)/(time scale for nitrogen adsorption). Both g and p reflect catalyst properties.

Other dimensionless time-constant ratios emerging from the analysis are

$$\alpha = \frac{L\varepsilon/v}{1/(k_n N_f)} = \frac{\text{fluid residence time}}{\text{time scale for N adsorption}}, \tag{C.7}$$

$$\gamma = \frac{L\varepsilon/v}{1/k_{HDN}} = \frac{\text{fluid residence time}}{\text{time scale for HDN reaction}}, \tag{C.8}$$

$$\eta = \frac{1/\text{WHSV}}{(1/k_s q_m)} = \frac{\text{space time}}{\text{time scale for achieving maximum S adsorption}}, \tag{C.9}$$

$$\mu = \frac{1/\text{WHSV}}{(1/k_n q_m)} = \frac{\text{space time}}{\text{time scale for achieving maximum N adsorption}}. \tag{C.10}$$

Note that α and γ may be related to a Damköhler number and $g = \alpha/\gamma$.

References

[1] M. Houalla, N.K. Nag, A.V. Sapre, D.H. Broderick, B.C. Gates, AIChE J. 24 (1978) 1015.
[2] M. Breysse, G. Djega-Mariadassou, S. Pessayre, C. Geantet, M. Vrinat, G. Pérot, M. Lemaire, Catal. Today 84 (2003) 129.
[3] X. Ma, K. Sakanishi, T. Isoda, I. Mochida, Paper Am. Chem. Soc. Prepr. Div. Petrol. Chem. 39 (1994) 622.
[4] T. Kabe, A. Ishihara, Q. Zhang, Appl. Catal. A 97 (1993) L1.
[5] V. Meille, E. Schulz, M. Lemaire, M. Vrinat, J. Catal. 170 (1997) 29.
[6] D.D. Whitehurst, T. Isoda, I. Mochida, Adv. Catal. 42 (1998) 345.
[7] M.J. Girgis, B.C. Gates, Ind. Eng. Chem. Res. 30 (1991) 2021.
[8] H. Topsøe, B.S. Clausen, F.E. Massoth, Hydrotreating Catalysis, Springer, New York, 1996.
[9] T. Kabe, A. Ishihara, W. Qian, Hydrodesulfurization and Hydrodenitrogenation, Wiley–VCH, New York, 1999.
[10] V. LaVopa, C.N. Satterfield, J. Catal. 100 (1988) 375.
[11] E. Furimsky, F.E. Massoth, Catal. Today 52 (1999) 381.
[12] I. Igniatiadis, M. Kuroki, P. Arpino, J. Chromatogr. 366 (1986) 251.
[13] J.M. Schmitter, I. Igniatiadis, M. Dorbon, P. Arpino, G. Guiochon, H. Toulhout, A. Huc, Fuel 63 (1984) 557.
[14] M. Dorbon, I. Igniatiadis, J.M. Schmitter, P. Arpino, G. Guiochon, H. Toulhout, A. Huc, Fuel 63 (1984) 565.
[15] G.C. Laredo, S. Leyva, R. Alvarez, M.T. Mares, J. Castillo, J.L. Cano, Fuel 81 (2002) 1341.
[16] P. Zeuthen, K.G. Knudsen, P.D. Whitehurst, Catal. Today 65 (2001) 307.
[17] S.D. Sumbogo Murti, H. Yang, K.H. Choi, Y. Korai, I. Mochida, Appl. Catal. A 252 (2003) 331.
[18] P. Wiwel, K. Knudsen, P. Zeuthen, D. Whitehurst, Ind. Eng. Chem. Res. 39 (2000) 533.
[19] T.C. Ho, J. Catal. 219 (2003) 442.
[20] T. Koltai, M. Macaud, A. Guevara, E. Schulz, M. Lemaire, R. Bacaud, M. Vrinat, Appl. Catal. A 231 (2002) 253.
[21] T.C. Ho, Catal. Rev.-Sci. Eng. 30 (1988) 117.
[22] H. Farag, D.D. Whitehurst, K. Sakanishi, I. Mochida, Catal. Today 50 (1999) 49.
[23] T. Kabe, K. Akamatsu, A. Ishihara, S. Otsuki, M. Godo, Q. Zhang, W. Qian, Ind. Eng. Chem. 36 (1997) 5146.
[24] T.C. Ho, Appl. Catal. A 244 (2003) 115.
[25] R. Aris, N.R. Amundson, in: Mathematical Methods in Chemical Engineering, vol. 2, Prentics Hall, NJ, 1973.
[26] F.E. Massoth, S.C. Kim, Catal. Lett. 57 (1999) 129.
[27] S.K. Bej, A.K. Dalai, J. Adjaye, Energy Fuels 15 (2001) 377.
[28] M.V. Landau, L. Vradman, M. Herkowitz, D. Yitzhaki, in: B. Delmon, G.F. Froment, P. Grange (Eds.), Hydrotreatment and Hydrocracking of Oil Fractions, Elsevier, Amsterdam, 1999.
[29] Q. Zhang, A. Ishihara, T. Kabe, Sekiyu Gakkaishi 39 (1996) 410.